Biomaterials Science

PAPER

View Article Online
View Journal | View Issue

Cite this: *Biomater. Sci.*, 2019, **7**, 2803

An eximious and affordable GSH stimulus-responsive poly(α-lipoic acid) nanocarrier bonding combretastatin A4 for tumor therapy

Zhilin Liu, [a,b,c] Na Shen,[a,c] Zhaohui Tang, *[a,c] Dawei Zhang,[a,c] Lili Ma,[a,c] Chenguang Yang[a,c] and Xuesi Chen *[a,c]

Received 2nd January 2019,
Accepted 1st April 2019

DOI: 10.1039/c9bm00002j

rsc.li/biomaterials-science

Due to poor penetration of cytotoxic-drug-loaded-nanomedicines, more and more attention has been paid to nanodrugs of vascular disrupting agents (VDAs). However, traditional VDA nanodrugs lack tumor-selectivity, so new nano-carriers for tumor-selective CA4 delivery are urgently needed. Here, a novel PEGylated poly(alpha-lipoic acid) graft combretastatin A4 (PALA-*g*-mPEG/CA4) nanoparticle with glutathione (GSH) stimulus responsive ability was prepared from alpha-lipoic acid in a simple approach, which can accumulate and release CA4 selectively in a tumor site. Furthermore, this simple system has potential application value for tumor-targeting delivery and GSH sensitive release of other drugs.

1. Introduction

Nanoparticles have poor penetration in solid tumors. Although the nano-carriers can deliver many anti-tumor agents to the periphery of tumors,[1–3] the loaded-drugs have difficulty in penetrating into the tumoral center. This phenomenon impairs the anti-tumor efficacy of many cytotoxic-drug-loaded-nanomedicines. Therefore, more and more attention has been paid to vascular disrupting agents (VDAs),[4] because the tumor tissue penetration is not necessary for VDAs to retard the tumor growth.[5] As we all know, the tumor vessel has a close relationship with the tumor growth, which is an attractive target for cancer therapy. The mechanism of VDAs[6] is by depolymerizing microtubules and destroying blood vessels, and then nutrients and oxygen supply are blocked, eventually leading to tumor necrosis. Combretastatin A4 (CA4) is a well-known leading compound as a vascular disrupting agent. As an inhibitor of tubulin polymerization, CA4 binds to the same site on tubulin as colchicines, which results in rapid tumor vascular shutdown, and then ischemia causes extensive centralized tumor necrosis to realize the treatment of tumors by a long-range strike as a consequence. However, CA4 is considered to be not suitable for intravenous injection for its poor water-solubility and short circulation half-life.[7]

In recent years, some kinds of nanoparticles based on CA4 have been prepared to achieve the prolonged half-life and enhance the anticancer effect.[8–10] For example, Liu *et al.*[11] designed a poly(L-glutamic acid)-combretastatin A4 conjugate to prolong the blood circulation time and improve the accumulation at the tumor site as well as the distribution around the tumor vessels, which markedly improved the therapeutic efficiency of CA4. But these VDA nanodrugs lack tumor-selectivity, and they widely distribute in normal organs after administration, which results in potential safety problems. So design of new nano-carriers with tumor-selective CA4 delivery is urgently required.

Stimuli-responsive nanoparticles have attractive advantages over traditional nanoparticles in tumor-selective drug delivery.[12] Based on the unique features of the tumor microenvironment like pH[13–16] and enzyme[17] differences, and high glutathione (GSH)[18,19] and reactive oxygen species (ROS)[20,21] levels, many different stimuli-responsive nano-carriers have been designed to achieve a high anti-tumor effect in drug delivery systems (DDS). These nano-carriers can not only enhance accumulation of drugs at tumor sites *via* the EPR effect but also release the drug in a tumor-selective manner. Of these stimuli, as the malignant tissues possess at least four-fold higher concentrations of GSH than normal tissues,[22–25] the intracellular GSH concentration (1–10 mM) in tumor cells is much higher than that in common fluids outside cells (20–40 μM),[26] such as plasma and other body fluids. Thus, the GSH-responsive nano-drugs have advantages in tumor accumulation, more release in tumor sites and realizing tumor selectivity.[27]

[a]*Key Laboratory of Polymer Ecomaterials, Changchun Institute of Applied Chemistry, Chinese Academy of Sciences, Changchun 130022, P. R. China.*
E-mail: xschen@ciac.ac.cn
[b]*University of Science and Technology of China, Hefei 230026, P. R. China*
[c]*Jilin Biomedical Polymers Engineering Laboratory, Changchun, 130022, P. R. China*

Herein, instead of the cumbersome synthesis steps of disulfide-containing nanoparticles needed in general,[28] alpha-lipoic acid, an ancient and cheap antioxidant as a monomer, was selected to prepare poly(alpha-lipoic acid) (PALA) by simple self-polymerization.[29,30] In order to obtain long circulation time *in vivo*, PALA was then modified through PEGylation to obtain a PEGylated poly(alpha-lipoic acid) copolymer (PALA-*g*-mPEG). After that, it was proposed to derive a PEGylated poly(alpha-lipoic acid) graft CA4 (PALA-*g*-mPEG/CA4) conjugate nanoparticle, realizing GSH sensitive disintegration, and CA4 liberating from the nanoparticles to recover its activity selectively in the tumor microenvironment (Fig. 1).

In brief, a novel GSH stimulus-responsive disulfide-containing CA4 nanoparticle from alpha-lipoic acid in a simple approach was first proposed, and its anti-tumor effect was verified compared to free CA4P. The data suggested that PALA-*g*-mPEG/CA4 has more advantages than small-molecule CA4P, expanding the potential applications of CA4 in the treatment of tumors.

2. Experimental

2.1 Materials

DL-Alpha-lipoic acid (ALA), poly(ethylene glycol) monomethyl ether (M_n = 5000 g mol^{-1}) ($mPEG_{5k}$), 1-ethyl-3-(3-dimethylaminopropyl)-carbodiimide hydrochloride (EDC·HCl), 4-dimethylaminopyridine (DMAP) and reduced L-glutathione (GSH) were purchased from Sigma-Aldrich LLC (Shanghai, China). Combretastatin A4 (CA4) and combretastatin-A4 phosphate (CA4P) were purchased from Hangzhou Great Forest Biomedical Ltd, China. Dulbecco's modified Eagle's medium (DMEM, Gibco) and fetal bovine serum (FBS, Gibco) were purchased from Thermo Fisher Scientific (Shanghai, China). All other reagents and solvents were purchased from Sinopharm Chemical Reagent Co., Ltd (Shanghai, China).

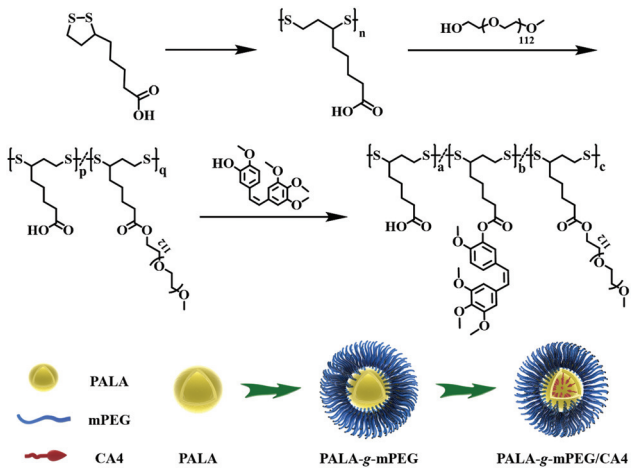

Fig. 1 Synthesis of PALA-*g*-mPEG/CA4.

2.2 Characterization

^{1}H NMR spectra were recorded on a Bruker AV 300 NMR spectrometer in d-DMSO. Number-, weight-average molecular weights (M_n, M_w) and molecular weight distributions (polydispersity index, PDI = M_w/M_n) were obtained by gel permeation chromatography (GPC) on a Waters 2414 system equipped with an Ultra hydrogel linear column and a Waters 2414 refractive index detector. The calibration of molecular weight was estimated with standard polystyrenes and DMF was used as an eluent with a flow velocity of 1.0 mL min^{-1} at 25 °C. The zeta potentials of the nanoparticles were measured by using a Zeta Potential/BI-90Plus particle size analyzer (Brookheaven Instruments Corporation, USA). Dynamic laser scattering (DLS) measurements were performed on a WyattQELS instrument with a vertically polarized HeNe laser (Dawn EOS, Wyatt Technology, USA). The scattering angle was fixed at 90°. The ultraviolet-visible (UV-vis) absorption spectrum was measured by using a UV-2401PC spectrophotometer (Shimadzu, Japan). The MTT assay was performed by using a microplate reader (INFINITE 200 PRO, USA). The fluorescence intensity was measured by using a Fluorescence Master System (Photon Technology International, USA). Multispectral optoacoustic tomography equipment (inVision 128) was from iThera Medical (Munich, Germany). The HPLC analyses were performed on a Waters 1525 system equipped with a reverse-phase column (Symmetry® C18). Elution was performed with acetonitrile and water (v/v = 4 : 1) pumped at a flow velocity of 1.0 mL min^{-1} at 25 °C.

2.3 Cell lines and animals

The murine breast cancer 4T1 cell line and human umbilical vein endothelial cell line (HUVEC) were purchased from Shanghai Bogoo Biotechnology Co. Ltd (China). SD rats (male, average body weight 220–250 g, 7–8 weeks old) were bought from Liaoning Changsheng Biotechnology Co., Ltd (Laioning, China). BALB/c mice (female, average body weight 17–19 g, 6–8 weeks old) and BALB/c nude mice (female, average body weight 18–20 g, 6–8 weeks old) were bought from Beijing Vital River Laboratory Animal Technology Co. Ltd (Beijing, China). The 4T1 tumor model was prepared by injecting 4T1 cells (1.5×10^6) into the right hind leg of Balb/c mice. All animal procedures were performed in accordance with the Guidelines for Care and Use of Laboratory Animals of Jilin University and experiments were approved by the Animal Ethics Committee of Jilin University.

2.4 Synthesis of PALA-*g*-mPEG/CA4 nanoparticles

PALA was obtained by self-polymerization above the melting point of ALA without any initiator. Specifically, ALA (4.00 g, 19.42 mmol) was added to a dry flask under nitrogen flow and stirred at 90 °C for 1.5 h. The crude product was dissolved in 50.0 mL of THF and slowly precipitated by sedimentation in 500 mL diethyl ether 2 times to obtain a sticky white solid. The THF and diethyl ether were removed under vacuum to obtain dry PALA (1.85 g, 46.3%).

Then, PALA (1.00 g) was dissolved in 30.0 mL THF. Meanwhile, $mPEG_{5k}$ (4.00 g, 0.80 mmol), EDC·HCl (229 mg, 1.20 mmol) and DMAP (36 mg, 0.30 mmol) were dissolved in 30.0 mL of DMSO, then mixed with PALA, and stirred for 48 h at room temperature. The reaction mixture was dialyzed using a dialysis bag (MWCO 7000 Da) against deionized water for 2 days. PALA-*g*-mPEG (3.36 g, 67.2%) was obtained after lyophilization.

Finally, CA4 was grafted to the prepared PALA-*g*-mPEG by Steglich esterification. PALA-*g*-mPEG (940 mg, 0.15 mmol), DMAP (36.6 mg, 0.30 mmol) and CA4 (286 mg, 1.00 mmol) were dissolved in 20.0 mL anhydrous DMF in a glass reactor, and then DIC (186 μL, 1.20 mmol) was added, and stirred for 24 h at room temperature. The reaction mixture was slowly precipitated into diethyl ether, re-dissolved in DMF, and dialyzed against distilled water. PALA-*g*-mPEG/CA4 was obtained after lyophilization. The drug loading content (DLC) and drug loading efficiency (DLE) of the PALA-*g*-mPEG/CA4 were determined by ultraviolet detector HPLC (UV-HPLC) analyses with a UV-Vis detector at 305 nm, and the elution was performed with acetonitrile and water (v/v = 4 : 1) pumped at a flow velocity of 1.0 mL min^{-1} at 25 °C:

$$\mathrm{DLC} = \frac{\text{weight of CA4 loaded in nanoparticles}}{\text{weight of CA4-loaded nanoparticles}} \times 100\%$$

$$\mathrm{DLE} = \frac{\text{weight of CA4 loaded in nanoparticles}}{\text{weight of feeding CA4}} \times 100\%.$$

2.5 Stability and GSH-responsiveness of PALA-*g*-mPEG/CA4

The stability and GSH-responsiveness of PALA-*g*-mPEG/CA4 were investigated in phosphate buffered saline solution (100 mM, pH 7.4) with or without 5 mM GSH, respectively. The particle sizes of PALA-*g*-mPEG/CA4 (0.15 mg mL^{-1}) were measured at 24 h by DLS and TEM.

2.6 *In vitro* release of CA4

In vitro release of CA4 from PALA-*g*-mPEG/CA4 nanoparticles was conducted using a dialysis method. Briefly, a phosphate buffered saline solution (100 mM, pH 7.4) and a phosphate buffered saline solution (100 mM, pH 7.4) containing GSH with predetermined concentrations (0.1, 1.0, 5.0 mM) were used as release media. PALA-*g*-mPEG/CA4 nanoparticles (3 mg) were dissolved in 3.0 mL different release media. The samples were transferred into dialysis bags (MWCO 3500 Da), shaking in 47.0 mL release media respectively with 80 rpm at 37 °C. At predetermined time points (1, 2, 4, 8, 12, 24, 36 and 48 h), 3.0 mL of outside solution was tested and next 3.0 mL fresh media was added. The accumulative release of CA4 was monitored by UV-HPLC analyses with a UV-Vis detector at 305 nm, and the elution was performed with acetonitrile and water (v/v = 4 : 1) pumped at a flow velocity of 1.0 mL min^{-1} at 25 °C, as described above.

2.7 Pharmacokinetics

Pharmacokinetics was characterized *via* measuring CA4 levels by collecting the eye arterial blood of SD female rats (200–250 g). Specifically, six rats were divided into two groups of 3 each, and they were injected with free CA4P (50.0 mg kg^{-1} on the basis of CA4) or PALA-*g*-mPEG/CA4 (50.0 mg kg^{-1} on the basis of CA4) *via* tail veins, respectively. Eye arterial blood was collected at predetermined times (5, 30, 60, 120, 240, 480, 720, 1440 min), and was heparinized and centrifuged to obtain plasma. Next, 150.0 μL of the plasma sample was deproteinized with 850.0 μL of methanol, vortexed for 15 min, and centrifuged at 8000 rpm for 10 min. 500 μL of the supernatant was collected, and dried up by pressured nitrogen at room temperature. The dried samples were dissolved in acetonitrile and water (v/v = 4 : 1) and filtered by using 0.22 μm filters before HPLC measurement. The pharmacokinetics assay of PALA-*g*-mPEG/CA4 and CA4P was performed by fluorescence detector HPLC (FLD-HPLC) with a fluorescence detector at 290 nm Ex and 390 nm Em, and the elution was performed with acetonitrile and water (v/v = 4 : 1) pumped at a flow velocity of 1.0 mL min^{-1} at 25 °C.

2.8 *In vitro* cytotoxicity of PALA-*g*-mPEG, CA4P and PALA-*g*-mPEG/CA4

We assessed the *in vitro* cytotoxicity of CA4P and PALA-*g*-mPEG/CA4 using the MTT assay. 4T1 or HUVEC cells were seeded in 96-well culture plates in 180 μL DMEM per well and allowed to adhere for 20 h. CA4P and PALA-*g*-mPEG/CA4 were dissolved in water to obtain 3.0 mM stock solution on the basis of CA4, and diluted from 3.0 mM by gradient dilution. Then 20 μL of the solutions were added to each hole and allowed to incubate for an additional 24 h. Next, 20 μL of MTT indicator dye (5 mg mL^{-1} in PBS, pH 7.4) was added to each well, and the cells were incubated for another 4 h at 37 °C in the dark. All the DMEM was emptied completely by adding 150 μL DMSO per well and shocked for 5 min. The absorbance of the solution was measured on the microplate reader at 490 nm. The relative cell viability was determined by comparing the absorbance of treated cells at 490 nm to non-treatment control wells. Data are presented as mean ± SD (n = 3).

2.9 Multispectral optoacoustic tomography imaging

Balb/c nude mice bearing 4T1 tumors at a volume of approximately 230 mm^3 were injected *via* tail veins with PALA-*g*-mPEG/CA4 at a dose of 50.0 mg kg^{-1} on the basis of CA4. At 24 h, the mice were anaesthetized with 2% isoflurane and placed into a multispectral optoacoustic tomography (MSOT) system to be imaged. Multispectral process (MSP) scanning was performed at 680, 715, 730, 760, 815, 850 and 900 nm. The results were reconstructed in a linear model and analyzed *via* linear regression.

2.10 CA4 accumulation in tumor

Balb/c mice bearing 4T1 tumors at a volume of approximately 150 mm^3 were injected *via* tail veins with PALA-*g*-mPEG/CA4 or CA4P at a dose of 50.0 mg kg^{-1} on the basis of CA4. The mice were sacrificed at 1 h, 4 h and 24 h after the injection (3 mice per group). The tumors were collected and homogenized in MeOH/H_2O and the clear suspensions were obtained by cen-

trifugation at 4 °C at 10 000 rpm for 10 min. Afterward, free CA4 concentrations were determined by using an FLD-HPLC system, as described above.

2.11 Immunohistochemical staining of CD31

BALB/c mice bearing 4T1 tumors at a volume of approximately 150 mm^3 were injected *via* tail veins with PBS, CA4P or PALA-*g*-mPEG/CA4 at a dose of 50.0 mg kg^{-1} on the basis of CA4. The mice were sacrificed after 48 h, and the tumors were excised. The obtained tumors were fixed in 4% (w/v) PBS-buffered paraformaldehyde for 72 h and embedded in paraffin. Paraffin-embedded tumors were prepared as serial sections (5 μm thick) and stained with CD31. Briefly, these fractions are in turn dewaxed and rehydrated with xylene, a series of graded ethanol, and deionized water. Endogenous peroxidase was quenched with 3% hydrogen peroxide (H_2O_2) for 10 min. Then the sliced samples were rinsed with deionized water, then dipped in boiled citric buffer for 15 min, and blocked with blocking buffer (5% normal goat serum) for 1 h, and then the slides were incubated with rabbit anti-CD31 (1 : 100) polyclonal antibody overnight at 4 °C. Next, goat anti-rabbit IgG (1 : 1000, abcam) was added and incubated at room temperature for 1 h after washing with PBS. The sections were stained with diaminobenzidine (DAB), counterstained with hematoxylin and mounted with mounting medium. The section stained brown partly represents CD31 positive.

2.12 Anticancer efficiency *in vivo*

A 4T1 tumor-bearing Balb/c mouse model was constructed by injection of 4T1 cancer cells (1.5×10^6 per mouse) on the right hind legs of Balb/c mice. The mice were randomly divided into 4 groups of 5 mice each as the tumors grew to about 120 mm^3. Then they were injected with PBS, blank PALA-*g*-mPEG (170.0 mg kg^{-1}, the amount was equal to the PALA-*g*-mPEG in PALA-*g*-mPEG/CA4 formulation), free CA4P (30.0 mg kg^{-1} on the basis of CA4) or PALA-*g*-mPEG/CA4 (30.0 mg kg^{-1} on the basis of CA4) *via* tail vein injection on days 0, 4, 8, 12 and 16. The tumor sizes and body weight were measured every other day, and the tumor volume (V; mm^3) was calculated as $V = a \times b^2/2$, where a and b (mm) were the longest and shortest diameter of tumors, respectively.

2.13 H & E staining

The mice were sacrificed two days after the last injection in the anti-tumor efficiency test. The major organs (heart, liver, spleen, lung, and kidney) and tumors were excised and fixed in 4% buffered formaldehyde (W/V) for 72 h, then embedded in paraffin, and sliced at 5 μm for haematoxylin and eosin staining (H & E).

2.14 Statistical analysis

Statistical analysis (n = 3) was expressed as the mean ± SD, using the Student's t-test. Differences were classified as significant ($p < 0.05$), very significant ($p < 0.01$) and extremely significant ($p < 0.001$).

3. Results and discussion

3.1 Preparation and characterization of PALA-*g*-mPEG/CA4

PALA was prepared by self-polymerization of the alpha-lipoic acid monomer at 90 °C for 1.5 h, and then characterized by ^{1}H NMR. As shown in Fig. 2, the $-CH_2-$ (a) protons of ALA display resonances at δ 3.13 and 3.18 ppm, and the $-CH_2-$ (b) protons of ALA show two peaks at δ 1.87 and 2.40 ppm, indicating the existence of the dithiolane ring. In ^{1}H NMR of PALA, the peaks of $-CH_2-$ (a) and (b) of ALA disappear, and the new wide peaks were observed at δ 2.81 ppm (a) and 1.93 ppm (b) instead, suggesting that the chemical bond tension decreased as the dithiolane ring of ALA opened, and PALA had been obtained as anticipated.

To further confirm that PALA was prepared successfully, the UV-Vis spectra of ALA and PALA were compared (Fig. 3A), and ALA showed a high ultraviolet absorption characteristic peak at 335 nm, but neither PALA nor PALA-*g*-mPEG has a peak at 335 nm, which offered evidence that PALA and PALA-*g*-mPEG were obtained, respectively.

PALA-*g*-mPEG was characterized by GPC analysis as shown in Fig. 3B. mPEG had a high peak at 20.2 min, but PALA-*g*-mPEG shows no peak there, indicating that mPEG has been successfully grafted onto the PALA chain, and the ungrafted mPEG does not exist in PALA-*g*-mPEG. The number average molecular weight (M_n) of PALA-*g*-mPEG is 14.9×10^3, while the polydispersity index (PDI, M_w/M_n) is 1.12.

The mPEG/PALA ratio in the PALA-*g*-mPEG was determined by ^{1}H NMR. The integral ratio of peak p and peak b in PALA-*g*-mPEG is about 45 : 1, indicating that the mass ratio of mPEG to PALA was about 5 : 1.

Then CA4 was grafted to PALA-*g*-mPEG and the product was purified by dialysis to remove free CA4 and other small-molecule impurities. To measure whether CA4 was grafted to PALA-

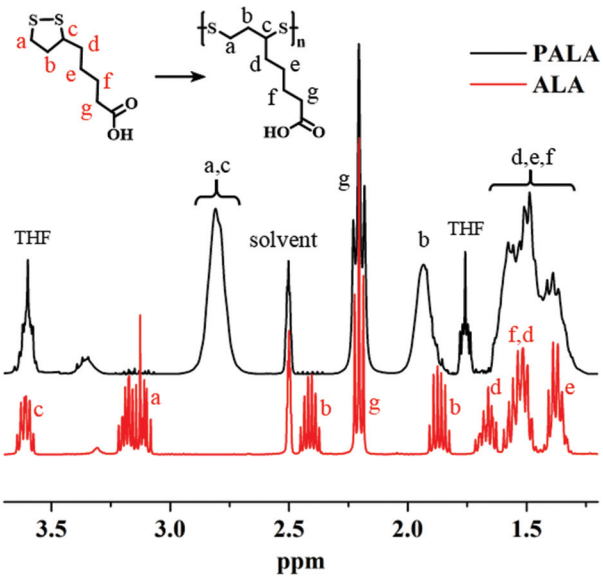

Fig. 2 ^{1}H NMR spectra of ALA and PALA.

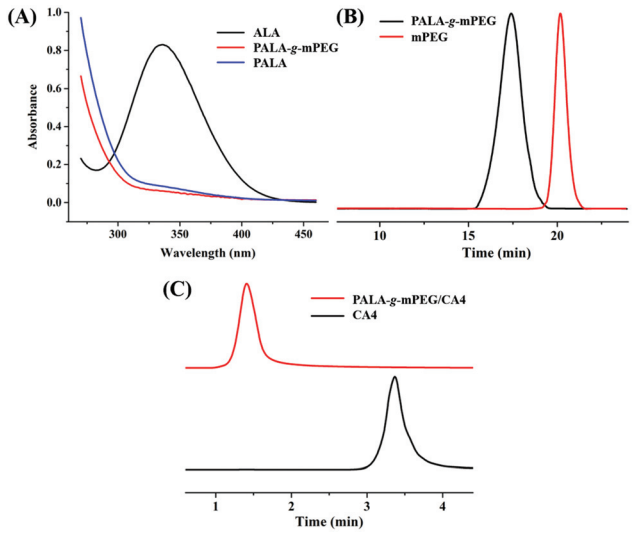

Fig. 3 (A) UV-vis spectra of ALA, PALA and PALA-*g*-mPEG; (B) GPC curves of PALA-*g*-mPEG and mPEG and (C) HPLC curves of CA4 and PALA-*g*-mPEG/CA4.

g-mPEG as expected, the freeze-dried product was characterized by ^{1}H NMR. The purity of PALA-*g*-mPEG/CA4 was determined by HPLC. As shown in Fig. 3C, the peak of free CA4 appeared at 3.43 min, while the peak of PALA-*g*-mPEG/CA4 appeared at 1.35 min without the peak at 3.43 min, indicating that the pure PALA-*g*-mPEG/CA4 without free CA4 was obtained.

As shown in Fig. 4, peaks j, i and h of PALA-*g*-mPEG/CA4 illustrated that CA4 was successfully grafted onto the PALA

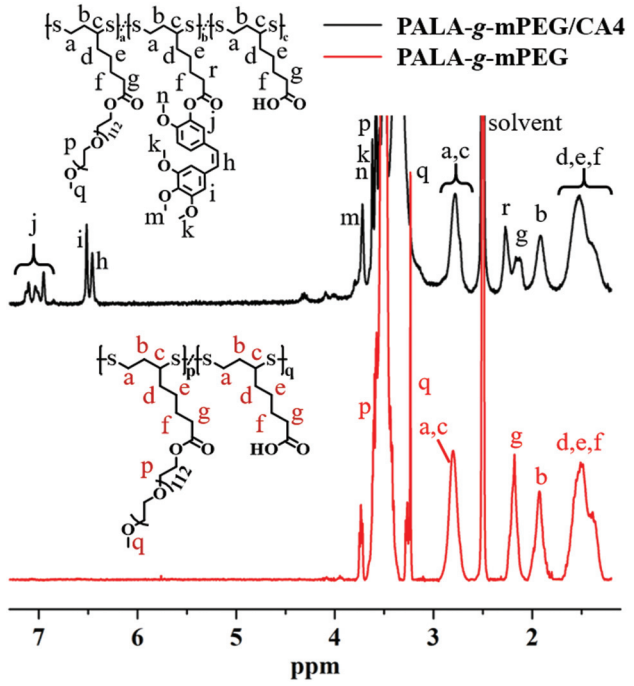

Fig. 4 ^{1}H NMR spectra of PALA-*g*-mPEG and PALA-*g*-mPEG/CA4.

chain. And the appearance of the new peak r indicated that the chemical environment of the hydrogen atoms at r had changed due to the conjugation of CA4, which also proved that CA4 had been successfully grafted. Through the integral ratio of peaks j, i, h and peak p, DLC was calculated to be 14.9 wt%.

The DLC and DLE of PALA-*g*-mPEG/CA4 were measured to be 14.3 wt% and 77%, respectively. The zeta potential of PALA-*g*-mPEG was negative 16.46 ± 4.77 mV, while the zeta potential of PALA-*g*-mPEG/CA4 increased to negative 8.95 ± 4.53 mV because CA4 had grafted to the side carboxyl group on PALA-*g*-mPEG.

3.2 Stability and GSH-responsiveness of PALA-*g*-mPEG/CA4

As the main chain of PALA-*g*-mPEG/CA4 is composed of disulfide bonds, obviously it has a sensitive response to GSH. To investigate the responsiveness, PALA-*g*-mPEG/CA4 was incubated with or without 5 mM GSH for 24 h. TEM (Fig. 5A and B) and DLS (Fig. 5C) results showed that PALA-*g*-mPEG/CA4 was stable in the absence of GSH, but the particle size of PALA-*g*-mPEG/CA4 changed irregularly in the presence of GSH, indicating that PALA-*g*-mPEG/CA4 would break the chain of disulfide bonds under the action of GSH and degrade at last, implying that after the accumulation of PALA-*g*-mPEG/CA4 in tumor tissue by the EPR effect, it would degrade and release the drug due to the higher GSH concentration at the tumor

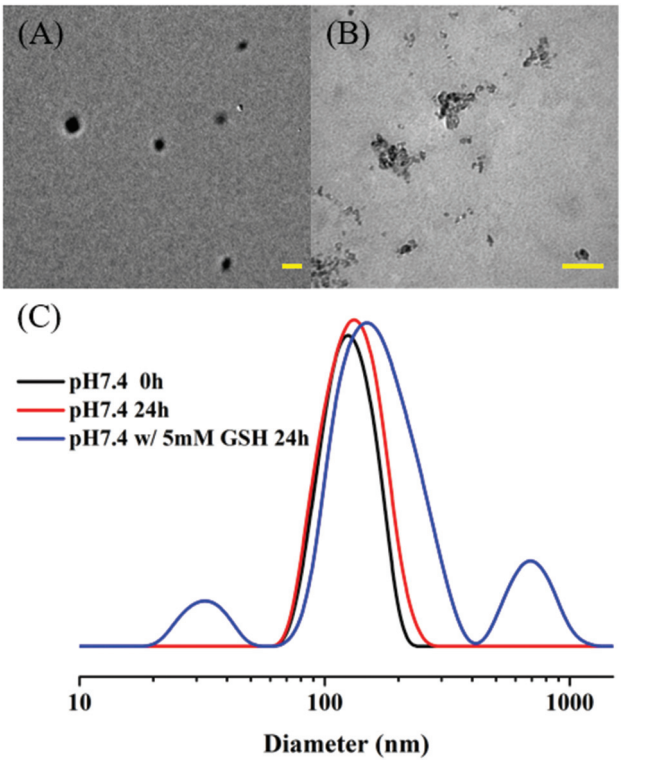

Fig. 5 The size changes of PALA-*g*-mPEG/CA4 under different conditions. (A) TEM image of PALA-*g*-mPEG/CA4 at PBS of pH 7.4 for 0 h; (B) TEM image of PALA-*g*-mPEG/CA4 at PBS of pH 7.4 with 5 mM GSH for 24 h; (C) DLS analysis of PALA-*g*-mPEG/CA4 size changes.

site, which can achieve more targeted delivery with less toxic side effects.

3.3 *In vitro* drug release

To investigate the impact of GSH on drug release of PALA-*g*-mPEG/CA4, we compare the release of PALA-*g*-mPEG/CA4 in different concentrations of GSH. As shown in Fig. 6A, with the change of GSH concentration from 0.1, 1.0 to 5.0 mM, the release of CA4 increased from 25.8%, 46.3% to 79.2% in 48 h, indicating that PALA-*g*-mPEG/CA4 can successfully realize degradation and release drugs at a high concentration of GSH to achieve specific release of CA4 in tumor tissue.

3.4 Pharmacokinetics

In order to compare the circulation time of PALA-*g*-mPEG/CA4 and CA4P *in vivo*, SD rats were administered with PALA-*g*-mPEG/CA4 or CA4P at a dose of 50.0 mg kg^{-1} on the basis of CA4. As shown in Fig. 6B, the plasma concentration time profiles fitted in two-compartment models well, and the main pharmacokinetic parameters of PALA-*g*-mPEG/CA4 were as follows: the Area Under Curve 0-*t* (AUC_{0-t}) 4089.24 ± 2178.15 mg L^{-1}, AUC_{0-inf} 4206.48 ± 2192.84 mg L^{-1}, $t_{1/2}$ α 0.36 ± 0.18 h, $t_{1/2}$ β 5.36 ± 0.0.47 h. In contrast, for free CA4P, AUC_{0-t} 98.99 ± 49.52 mg L^{-1}, AUC_{0-inf} 113.99 ± 51.18 mg L^{-1}, $t_{1/2}$ α 0.10 ± 0.01 h, and $t_{1/2}$ β 1.54 ± 0.31 h. The pharmacokinetic data indicate that PALA-*g*-mPEG/CA4 has a longer blood circulation time than CA4P, achieving more tumor accumulation and retention to destroy tumor blood vessels for a longer period of time, which can provide higher anti-tumor efficacy by administering lower doses at longer intervals. Pharmacokinetic data were analyzed using Drug and Statistics (DAS) software version 3.1.6.

3.5 *In vitro* cytotoxicity of PALA-*g*-mPEG, CA4P and PALA-*g*-mPEG/CA4

To understand the cytotoxicity of the prepared materials and CA4, 4T1 and HUVEC cells were seeded for MTT assay. As shown in Fig. 7, the results showed that CA4 exhibits cytotoxicity to vascular endothelial cells, but has little effect on 4T1, and due to the sustained release of PALA-*g*-mPEG/CA4, the cytotoxicity of PALA-*g*-mPEG/CA4 was reduced. Meanwhile, the prepared material, PALA-*g*-mPEG, shows no cytotoxicity to both cells, which means that PALA-*g*-mPEG can be used as an excellent drug carrier.

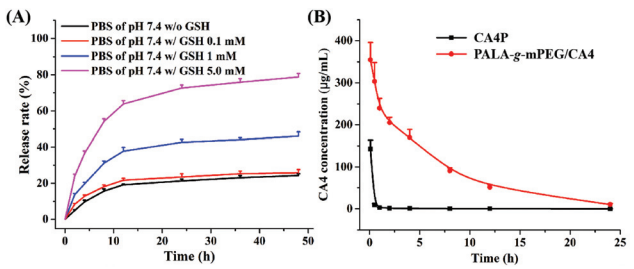

Fig. 6 (A) Accumulative release rate of CA4 under different conditions and (B) pharmacokinetics of CA4P and PALA-*g*-mPEG/CA4.

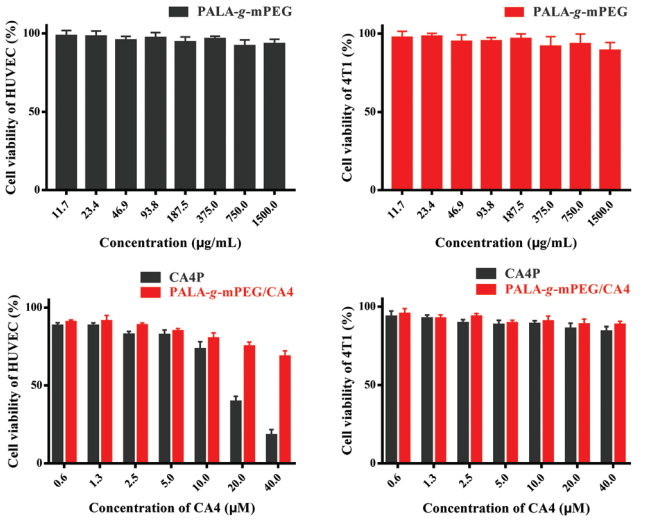

Fig. 7 The cytotoxicity of PALA-*g*-mPEG to (A) HUVEC and (B) 4T1, and the cytotoxicity of CA4P and PALA-*g*-mPEG/CA4 to (C) HUVEC and (D) 4T1.

3.5 Multispectral optoacoustic tomography

We further compared the tumor hypoxia conditions before and after the treatment of PALA-*g*-mPEG/CA4. As shown in Fig. 8, after the treatment with PALA-*g*-mPEG/CA4 for 24 h, the ratio of HB/HBO_2 at the tumor site was 2.33 fold that without treatment (HB: hemoglobin; HBO2: oxyhemoglobin), due to the extensive tumor necrosis in Balb/c nude mice with 4T1 tumors, demonstrating that PALA-*g*-mPEG/CA4 achieved great tumor accumulation and responsive release of CA4, and indicating that many blood vessels inside the tumor were narrowed or blocked.

3.6 CA4 accumulation in tumors

To demonstrate that PALA-*g*-mPEG/CA4 achieved better tumor site accumulation than CA4P directly, the concentrations of CA4 in tumors at 1 h, 4 h and 24 h were calculated after the injection of CA4P and PALA-*g*-mPEG/CA4. As shown in Fig. 9, we can realize that PALA-*g*-mPEG/CA4 achieved much higher accumulation and more sustainable residence time than free CA4P, which provided a convincing reason to speculate that an improved anti-tumor effect should be obtained.

3.7 Immunohistochemistry of CD31

Immunohistochemistry staining was performed to show the vascular disruption in the tumor site (Fig. 10). Obviously, because of the destructive effect of CA4 on blood vessels, vessel density at the tumor site after CA4P treatment was much lower than that in the PBS group, while the blood vessel density after PALA-*g*-mPEG/CA4 treatment was the least. This is because CA4P only causes temporary blockade of blood vessels,[11] while the long retention time and continuous CA4

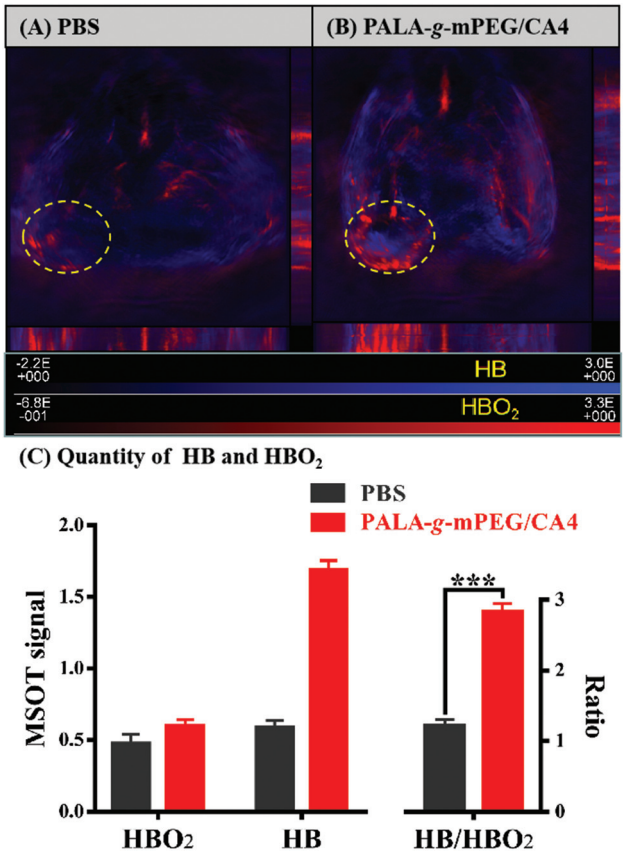

Fig. 8 Tumor hypoxia conditions after being administrated with (A) PBS or (B) PALA-*g*-mPEG/CA4 by multispectral optoacoustic tomography, and (C) the quantity of HB, HBO_2 and the ratio of HB/HBO_2 in the 4T1 tumors of Balb/c nude mice.

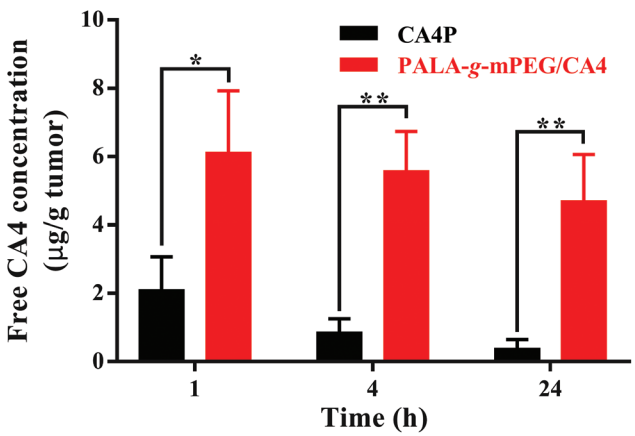

Fig. 9 The CA4 concentration in 4T1 tumors at 1 h, 4 h and 24 h after the injection of PALA-*g*-mPEG/CA4 or CA4P (50.0 mg kg^{-1} on the basis of CA4, $n = 3$, $^*p < 0.05$, $^{**}p < 0.01$).

release from PALA-*g*-mPEG/CA4 in the tumor site cause persistent blockade of blood vessels, which blocks the nutrient and oxygen supply of tumors, also exhibiting potential improvement for the therapeutic effect of tumors.

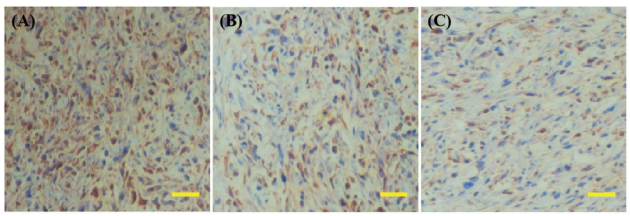

Fig. 10 Immunohistochemical staining of CD31 after 48 h treatment of (A) PBS, (B) CA4P or (C) PALA-*g*-mPEG/CA4. Scale bar: 50 μm.

3.8 Anti-tumor efficiency *in vivo*

Because of the above encouraging results, we further compared the anti-tumor efficiency of CA4P and PALA-*g*-mPEG/CA4 *in vivo*. As shown in Fig. 11, there were no significant differences in the tumor size and body weight change between the PBS group and the PALA-*g*-mPEG group, which indicated that blank PALA-*g*-mPEG had no anti-tumor effect. Because of frequent administration, the CA4P group also showed a certain anti-tumor effect with 64.3% inhibition rate, but the tumor volume of the CA4P group still increased significantly, for CA4P it was easily cleared from the blood circulation system and there was no tumor enrichment. In contrast, the PALA-*g*-mPEG/CA4 group had a significant anti-tumor effect *via* its high tumor accumulation, selective drug release at the tumor site, and longer circulation time *in vivo*. The tumor inhibition rate was 83.1%.

3.9 H & E staining

At the end of the anti-tumor efficiency experiment, in order to further evaluate the therapeutic effects and toxicity of PALA-*g*-mPEG/CA4, the tumors and major organs were collected and stained with H & E for pathological analysis. For H & E staining (Fig. 12 and 13), the tumors treated with PBS had large nuclei

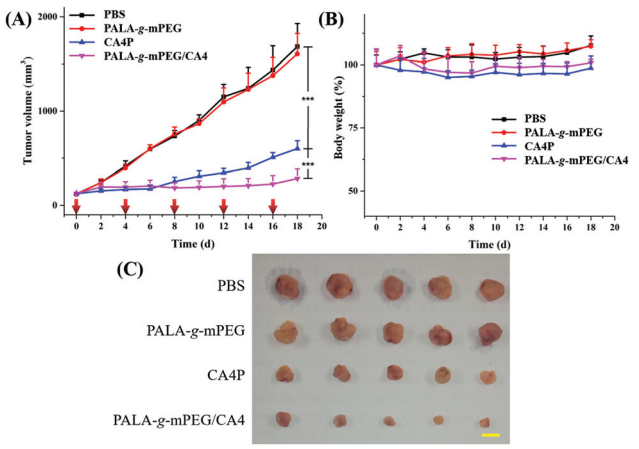

Fig. 11 Anticancer efficiency and body weight changes *in vivo*. (A) Tumor volume changes of the anti-tumor efficiency and injection schedule for all groups (arrows); (B) body weight changes of anti-tumor efficiency; (C) tumor images at the end of treatment. Scale bar: 10 mm. $n = 5$, $^{***}p < 0.001$.

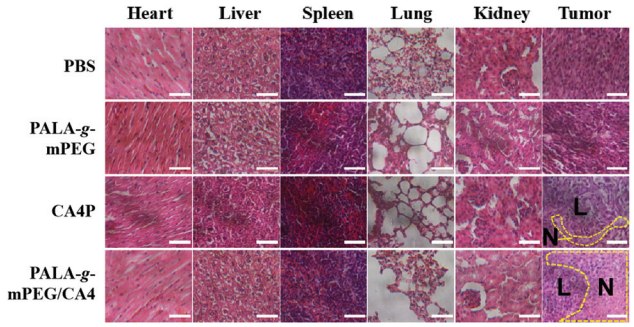

Fig. 12 H & E assay of mouse organs and tumors after treatment with PBS, PALA-*g*-mPEG, CA4P and PALA-*g*-mPEG/CA4. L and N indicate the live and necrotic regions. Scale bar: 50 μm.

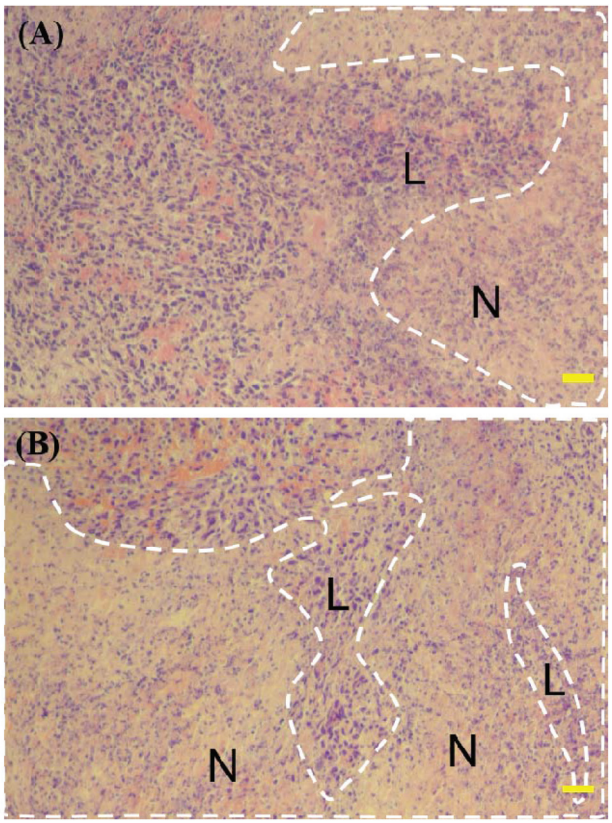

Fig. 13 Large tumor H & E images after the treatment of (A) free CA4P or (B) PALA-*g*-mPEG/CA4. L and N indicate the live and necrotic regions. Scale bar: 100 μm.

and more chromatin, revealing the powerful ability of tumor cell proliferation. There were no significant lesions and metastases in the normal organs of all four groups of mice. CA4P caused finite necrosis in the tumor (area covered with yellow lines of CA4P), and only the PALA-*g*-mPEG/CA4 group caused severe necrosis (area covered with yellow lines of PALA-*g*-mPEG/CA4), which indicated that PALA-*g*-mPEG/CA4 caused tumor internal necrosis by continuously destroying the internal blood vessels to achieve an excellent anti-tumor effect.

4. Conclusions

A novel GSH-responsive nano-carrier, PALA-*g*-mPEG, was developed in a simple way to achieve stability under physiological conditions and degradation in the presence of GSH. CA4 was bonded to the PALA-*g*-mPEG to obtain a new nanomedicine with long blood circulation time and high GSH stimulus-sensitivity. PALA-*g*-mPEG/CA4 achieved high anti-tumor activity to 4T1 breast cancer, which caused extensive tumor inner necrosis to realize the treatment of a tumor by a long-range strike.

Conflicts of interest

There are no conflicts to declare.

Acknowledgements

This work was financially supported by Ministry of Science and Technology of China (Project 2016YFC1100701 and 2018ZX09711003-012), the National Natural Science Foundation of China (Projects 51503202, 51673185, 51673189, 81702327 and 51390484), the Science and Technology Service Network Initiative (Project KFJ-SW-STS-166) and the Program of Scientific Development of Jilin Province (No. 20170101100JC).

Notes and references

1 Z. P. Guo, X. Z. Zhou, M. Z. Xu, H. Y. Tian, X. S. Chen and M. W. Chen, Dimeric camptothecin-loaded RGD-modified targeted cationic polypeptide-based micelles with high drug loading capacity and redox-responsive drug release capability, *Biomater. Sci.*, 2017, **5**(12), 2501–2510.
2 T. Wu, M. Tan, H. Y. Gong, Y. Wang and X. T. Shuai, Co-delivery of Andrographolide and Notch1-targeted siRNA to Macrophages with Polymer-based Nanocarrier for Enhanced Anti-inflammation, *Chin. J. Polym. Sci.*, 2018, **36**(12), 1312–1320.
3 J. Xie, X. Li, C. J. Jiang, R. J. G. Lee, Y. L. Zhou and L. S. Teng, Novel PLGA microspheres for sustained delivery of antisense oligonucleotide, *Chem. Res. Chin. Univ.*, 2013, **29**(5), 1003–1005.
4 M. M. Shenoi, I. Iltis, J. Choi, N. A. Koonce, G. J. Metzger, R. J. Griffin and J. C. Bischof, Nanoparticle Delivered Vascular Disrupting Agents (VDAs): Use of TNF-Alpha Conjugated Gold Nanoparticles for Multimodal Cancer Therapy, *Mol. Pharm.*, 2013, **10**(5), 1683–1694.
5 A. Hasani and N. Leighl, Classification and Toxicities of Vascular Disrupting Agents, *Clin. Lung Cancer*, 2011, **12**(1), 18–25.
6 A. Close, Antiangiogenesis and vascular disrupting agents in cancer: circumventing resistance and augmenting their therapeutic utility, *Future Med. Chem.*, 2016, **8**(4), 443–462.

7 R. Nallamothu, G. C. Wood, C. B. Pattillo, R. C. Scott, M. F. Kiani, B. M. Moore and L. A. Thoma, A tumor vasculature targeted liposome delivery system for combretastatin A4: Design, characterization, and in vitro evaluation, *AAPS PharmSciTech*, 2006, **7**(2), E7–E16.

8 W. T. Song, Z. H. Tang, D. W. Zhang, X. Wen, S. X. Lv, Z. L. Liu, M. X. Deng and X. S. Chen, Solid Tumor Therapy Using a Cannon and Pawn Combination Strategy, *Theranostics*, 2016, **6**(7), 1023–1030.

9 W. T. Song, Z. H. Tang, D. W. Zhang, H. Y. Yu and X. S. Chen, Coadministration of Vascular Disrupting Agents and Nanomedicines to Eradicate Tumors from Peripheral and Central Regions, *Small*, 2015, **11**(31), 3755–3761.

10 A. P. Subramanian, S. K. Jaganathan, A. Manikandan, K. N. Pandiaraj, N. Gomathi and E. Supriyanto, Recent trends in nano-based drug delivery systems for efficient delivery of phytochemicals in chemotherapy, *RSC Adv.*, 2016, **6**(54), 48294–48314.

11 T. Z. Liu, D. W. Zhang, W. T. Song, Z. H. Tang, J. M. Zhu, Z. M. Ma, X. D. Wang, X. S. Chen and T. Tong, A poly(L-glutamic acid)-combretastatin A4 conjugate for solid tumor therapy: Markedly improved therapeutic efficiency through its low tissue penetration in solid tumor, *Acta Biomater.*, 2017, **53**, 179–189.

12 S. Ganta, H. Devalapally, A. Shahiwala and M. Amiji, A review of stimuli-responsive nanocarriers for drug and gene delivery, *J. Controlled Release*, 2008, **126**(3), 187–204.

13 M. Q. Li, W. T. Song, Z. H. Tang, S. X. Lv, L. Lin, H. Sun, Q. S. Li, Y. Yang, H. Hong and X. S. Chen, Nanoscaled Poly (L-glutamic acid)/Doxorubicin-Amphiphile Complex as pH-responsive Drug Delivery System for Effective Treatment of Nonsmall Cell Lung Cancer, *ACS Appl. Mater. Interfaces*, 2013, **5**(5), 1781–1792.

14 J. Z. Du, X. J. Du, C. Q. Mao and J. Wang, Tailor-Made Dual pH-Sensitive Polymer-Doxorubicin Nanoparticles for Efficient Anticancer Drug Delivery, *J. Am. Chem. Soc.*, 2011, **133**(44), 17560–17563.

15 J. Z. Du, T. M. Sun, W. J. Song, J. Wu and J. Wang, A Tumor-Acidity-Activated Charge-Conversional Nanogel as an Intelligent Vehicle for Promoted Tumoral-Cell Uptake and Drug Delivery, *Angew. Chem., Int. Ed.*, 2010, **49**(21), 3621–3626.

16 J. Liu, S. Iqbal, X. J. Du, Y. Y. Yuan, X. Z. Yang, H. J. Li and J. Wang, Ultrafast charge-conversional nanocarrier for tumor-acidity-activated targeted drug elivery, *Biomater. Sci.*, 2018, **6**(2), 350–355.

17 P. D. Thornton, R. J. Mart and R. V. Ulijn, Enzyme-responsive polymer hydrogel particles for controlled release, *Adv. Mater.*, 2007, **19**(9), 1252–1256.

18 M. R. Elzes, N. Akeroyd, J. F. J. Engbersen and J. M. J. Paulusse, Disulfide-functional poly(amido amine)s with tunable degradability for gene delivery, *J. Controlled Release*, 2016, **244**, 357–365.

19 F. Yuan, J. L. Li, H. Cheng, X. Zeng and X. Z. Zhang, A redox-responsive mesoporous silica based nanoplatform for in vitro tumor-specific fluorescence imaging and enhanced photodynamic therapy, *Biomater. Sci.*, 2017, **6**(1), 96–100.

20 C. Tapeinos and A. Pandit, Physical, Chemical, and Biological Structures based on ROS-Sensitive Moieties that are Able to Respond to Oxidative Microenvironments, *Adv. Mater.*, 2016, **28**(27), 5553–5585.

21 D. Q. Chen, G. Q. Zhang, R. M. Li, *et al.*, Biodegradable, Hydrogen Peroxide, and Glutathione Dual Responsive Nanoparticles for Potential Programmable Paclitaxel Release, *J. Am. Chem. Soc.*, 2018, **140**(24), 7373–7376.

22 Z. Z. Huang, C. J. Chen, Z. H. Zeng, H. P. Yang, J. Oh, L. X. Chen and S. C. Lu, Mechanism and significance of increased glutathione level in human hepatocellular carcinoma and liver regeneration, *FASEB J.*, 2001, **15**(1), 19–21.

23 R. R. Perry, J. Mazetta, M. Levin and S. C. Barranco, Glutathione Levels and Variability in Breast-Tumors and Normal Tissue, *Cancer*, 1993, **72**(3), 783–787.

24 P. Zhang, J. L. Wu, F. M. Xiao, D. J. Zhao and Y. X. Luan, Disulfide bond based polymeric drug carriers for cancer chemotherapy and relevant redox environments in mammals, *Med. Res. Rev.*, 2018, **38**(5), 1485–1510.

25 C. R. Wolf, A. D. Lewis, J. Carmichael, D. J. Adams, S. G. Allan and D. J. Ansell, The Role of Glutathione in Determining the Response of Normal and Tumor-Cells to Anticancer Drugs, *Biochem. Soc. Trans.*, 1987, **15**(4), 728–730.

26 T. Schnelldorfer, S. Gansauge, F. Gansauge, S. Schlosser, H. G. Beger and A. K. Nussler, Glutathione depletion causes cell growth inhibition and enhanced apoptosis in pancreatic cancer cells, *Cancer*, 2000, **89**(7), 1440–1447.

27 M. H. Lee, Z. Yang, C. W. Lim, Y. H. Lee, S. Dongbang, C. Kang and J. S. Kim, Disulfide-Cleavage-Triggered Chemosensors and Their Biological Applications, *Chem. Rev.*, 2013, **113**(7), 5071–5109.

28 J. J. Nie, B. K. Qiao, S. Duan, C. Xu, B. Y. Chen, W. J. Hao, B. R. Yu, Y. L. Li, J. Du and F. J. Xu, Unlockable Nanocomplexes with Self-Accelerating Nucleic Acid Release for Effective Staged Gene Therapy of Cardiovascular Diseases, *Adv. Mater.*, 2018, **30**(31), 1–11.

29 A. Kisanuki, Y. Kimpara, Y. Oikado, N. Kado, M. Matsumoto and K. Endo, Ring-Opening Polymerization of Lipoic Acid and Characterization of the Polymer, *J. Polym. Sci., Part A: Polym. Chem.*, 2010, **48**(22), 5247–5253.

30 H. Ishida, A. Kisanuki and K. Endo, Ring-Opening Polymerization of Aromatic 6-Membered Cyclic Disulfide and Characterization of the Polymer, *Polym. J.*, 2009, **41**(2), 110–117.